ELSEVIER

Simulation of vortex shedding past a square cylinder near a wall

Gerhard Bosch* **and Wolfgang Rodi**
Institute for Hydromechanics, University of Karlsruhe, Karlsruhe, Germany

Calculations are reported for the flow past a square cylinder at Re=22,000 placed at various distances from an adjacent wall, including the limiting case without wall influence. Experiments have indicated that unsteady vortex shedding is suppressed when the wall is relatively close to the cylinder. Two-dimensional (2-D) unsteady equations are solved which allow any periodic shedding motion to be resolved; the superimposed turbulent fluctuations are simulated with two versions of the k-ε turbulence model: the standard k-ε model and the modification attributable to Kato and Launder (1993), which eliminates the excessive turbulent kinetic energy production in stagnation regions produced by the standard model. Wall functions are used with both versions. The standard model was found to damp the shedding motion unrealistically so that shedding was suppressed at considerably larger gap widths than observed experimentally. The Kato–Launder modification yields reasonable predictions over the full range of gap widths; for $G_w/D=0.75$ a quantitative comparison is presented with the authors' phase-resolved experiments, which shows fairly good accord.

Keywords: numerical simulations; turbulence models; vortex shedding; wall influence

Introduction

Periodic vortex shedding past slender bluff bodies occurs in many engineering and environmental flow situations. The shedding causes dynamic loading on the bodies and enhanced mixing in the wakes. Therefore, prediction of these phenomena is of great practical importance. A particular situation is the flow past a cylindrical structure placed near a wall as occurs in the flow past pipelines near the ground or past heat exchanger tubes near walls. The vicinity of a wall can have a distinct influence on the shedding, as has been shown in a number of experiments: no shedding is observed when the gap between the wall and the cylinder is below a certain distance. In this paper, the flow past long square cylinders near a wall is considered (see flow configurations sketched in Figure 1). Experiments on this configuration were carried out by Durao et al. (1991) and by the authors. Durao et al. found the critical value for the gap beyond which vortex shedding occurs to be in the range $G_w/D = 0.25 - 0.5$ at Re = 13,600. In our own experiments at Re = 22,000, steady flow was observed for $G_w/D = 0.25$, while vortex shedding was observed for $G_w/D \geq 0.5$. At $G_w/D = 0.375$ an intermediate flow behaviour was obtained.

In numerical simulations, the occurrence of shedding and the quality of the shedding prediction depend strongly on the turbulence model used and to some extent also on the numerical details. This was shown first for a square cylinder remote from walls by Franke and Rodi (1993). The standard k-ε model was found to underpredict severely the strength of the shedding motion, mainly because of the excessive turbulent kinetic energy production in the stagnation region. Reynolds-stress models avoid this problem and so does the Kato-Launder (1993) modification of the k-ε model. Both yield significantly improved predictions for the square-cylinder shedding flow.

Because of its dual flow behaviour; i.e., shedding occurring for larger gaps but not for smaller ones, the flow configuration shown in Figure 1 is a good test case for turbulence models, in particular for testing the improvements that the Kato-Launder (hereafter referred to as KaLa) modification to the standard k-ε model may bring. For this reason, calculations with both model versions—the standard k-ε model and the KaLa modification were carried out for various gap widths G_w/D and are presented here and compared with our own experiments. It is shown that the KaLa modification gives considerably more realistic results compared to the standard k-ε model also for shedding under the influence of a wall. For the limiting case without this influence, the results agree closely to those obtained by Kato and Launder (1993). The present experiments comprising visualisation studies and detailed phase-resolved laser Doppler velocimeter (LDV) measurements for $G_w/D = 0.75$, are also introduced briefly.

Address reprint requests to Prof. W. Rodi, Institute for Hydromechanics, University of Karlsruhe, Kaiserstrasse 12, 76128 Karlsruhe, Germany.
* Present Address: Laboratoire de Mécanique des Fluides URA CNRS 1217, Ecole Centrale de Nantes, 1 rue de la Noë, F-44072 Nantes Cedex 03, France.

Received 26 October 1995; accepted 29 February 1996

Int. J. Heat and Fluid Flow 17: 267–275, 1996

655 Avenue of the Americas, New York, NY 10010

0142-727X/96/$15.00
PII S0142-727X(96)00033-3

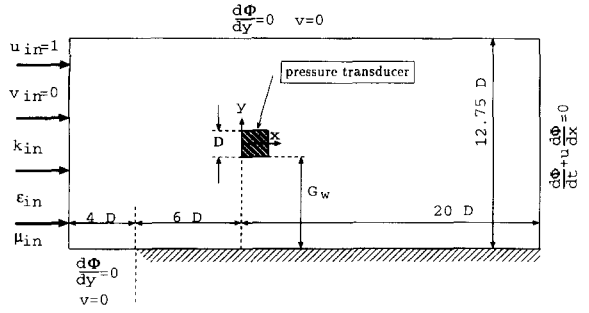

Figure 1 Computational domain and boundary conditions

Calculation method

Mean flow equations

At the higher Reynolds numbers considered here, stochastic three-dimensional (3-D) turbulent fluctuations are superimposed on the mainly two-dimensional (2-D) periodic vortex-shedding motion behind a cylinder. An instantaneous quantity Φ can, therefore, be separated into

$$\Phi = \langle\Phi\rangle + \Phi' \qquad \text{with} \qquad \langle\Phi\rangle = \overline{\Phi} + \tilde{\Phi} \tag{1}$$

where $\overline{\Phi}$ is the time mean value, $\langle\Phi\rangle$ the ensemble-averaged value, $\tilde{\Phi}$ the periodic fluctuation, and Φ' the stochastic turbulent fluctuation. In the calculations presented here, 2-D equations governing the temporal and spatial variation of the ensemble-averaged velocity components and pressure are solved. These are the ensemble-averaged continuity and momentum equations, which in tensor notation read as follows:

$$\frac{\partial\langle u_i\rangle}{\partial x_i} = 0 \tag{2}$$

$$\frac{\partial\langle u_i\rangle}{\partial t} + \frac{\partial[\langle u_l\rangle\langle u_i\rangle]}{\partial x_l} = -\frac{1}{\rho}\frac{\partial\langle p\rangle}{\partial x_i} + \frac{\partial}{\partial x_l}\left[\nu\frac{\partial\langle u_i\rangle}{\partial x_l} - \langle u_l' u_i'\rangle\right] \tag{3}$$

The Reynolds-stresses $\langle u_l' u_i'\rangle$ appearing in the momentum equations need to be simulated by a statistical turbulence model.

Turbulence models

Two high-Re versions of the k-ε model are used in connection with wall functions to determine the Reynolds-stresses $\langle u_l' u_i'\rangle$. Both employ the eddy-viscosity concept and relate the eddy-viscosity $\langle\nu_t\rangle$ to the turbulent kinetic energy $\langle k\rangle$ and its rate of dissipation $\langle\epsilon\rangle$. The quantities $\langle k\rangle$ and $\langle\epsilon\rangle$ are determined from the following model transport equations:

$$\frac{\partial\langle k\rangle}{\partial t} + \frac{\partial[\langle u_l\rangle\langle k\rangle]}{\partial x_l} = \frac{\partial}{\partial x_l}\left(\frac{\langle\nu_t\rangle}{\sigma_k}\frac{\partial\langle k\rangle}{\partial x_l}\right) + P_k - \langle\varepsilon\rangle \tag{4}$$

$$\frac{\partial\langle\varepsilon\rangle}{\partial t} + \frac{\partial[\langle u_l\rangle\langle\varepsilon\rangle]}{\partial x_l} = \frac{\partial}{\partial x_l}\left(\frac{\langle\nu_t\rangle}{\sigma_\varepsilon}\frac{\partial\langle\varepsilon\rangle}{\partial x_l}\right) + C_{\varepsilon 1}P_k\frac{\langle\varepsilon\rangle}{\langle k\rangle} - C_{\varepsilon 2}\frac{\langle\varepsilon\rangle^2}{\langle k\rangle} \tag{5}$$

The standard version of the k-ϵ model calculates the production P_k of $\langle k\rangle$ from

$$P_k = c_\mu\langle\varepsilon\rangle S^2,\ S \equiv \frac{\langle k\rangle}{\langle\varepsilon\rangle}\sqrt{\frac{1}{2}\left[\frac{\partial\langle u_i\rangle}{\partial x_j} + \frac{\partial\langle u_j\rangle}{\partial x_i}\right]^2} \tag{6}$$

To reduce the excessive production of $\langle k\rangle$ in stagnation regions (e.g., in front of a cylinder) due to an unrealistic simulation of the normal turbulent stresses in eddy-viscosity models, Kato and Launder (1993) proposed to replace the production expression in Equation 6 by

$$P_k = c_\mu\langle\varepsilon\rangle S\Omega,\ \Omega \equiv \frac{\langle k\rangle}{\langle\varepsilon\rangle}\sqrt{\frac{1}{2}\left[\frac{\partial\langle u_i\rangle}{\partial x_j} - \frac{\partial\langle u_j\rangle}{\partial x_i}\right]^2} \tag{7}$$

The quantity Ω is a rotation parameter. In simple shear flows, S and Ω are equal, but in stagnation flows $\Omega \approx 0$ and $S > 0$, resulting in the desired reduction of the k-production. The

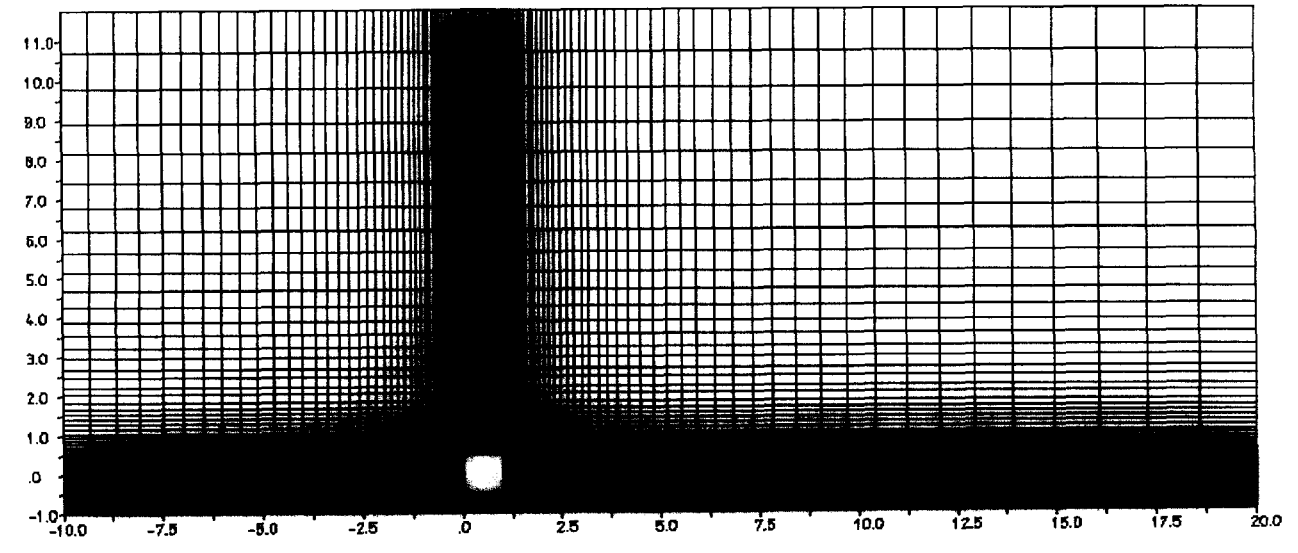

Figure 2 106 × 75 mesh for $G_w/D = 0.5$

Table 1 Mean drag coefficient $\overline{c_D}$ and Strouhal number Str for a quadratic cylinder remote from wall

Author	Model	$\overline{c_D}$	Str
Present	Standard k-ε+WF	1.618	0.126
Kato/Launder (1993)	Standard k-ε+WF	1.660	0.127
Present	Kato/Launder mod.+WF	2.108	0.146
Kato/Launder	Kato/Launder mod.+WF	2.050	0.145
	Experiments (For a range of Re)	2.05 – 2.23	0.135 – 0.139

standard values of the empirical constants are used in both versions ($c_\mu = 0.09$, $C_{\varepsilon 1} = 1.44$, $C_{\varepsilon 2} = 1.92$, $\sigma_k = 1.0$, $\sigma_\varepsilon = 1.3$).

Kato and Launder (1993) obtained significantly improved predictions with their modification for the square cylinder without the influence of a wall, a result that is confirmed by the present work.

Numerical solution procedure

The differential equations introduced above were solved numerically with an iterative finite-volume method whose basic features are described in Majumdar et al. (1989). The method uses a nonstaggered grid and Cartesian velocity components, handles the pressure-velocity coupling with the SIMPLEC algorithm (Van Doormal and Raithby 1984), employs the special momentum interpolation method of Rhie and Chow (1983) and solves the resulting system of difference equations iteratively with a tridiagonal-matrix algorithm. For spatial discretization, the HLPA (hybrid linear/parabolic approximation) scheme of Zhu (1991) is used, which combines a second-order upstream-weighted approximation with a first-order upwind-differencing scheme under the control of a convection-boundedness criterion. A first-order accurate fully implicit method was used for time discretization in connection with a relatively small time-step $\Delta t^* = \Delta t u_\infty / D = 0.02$. This gave virtually the same accuracy as a second-order three-level implicit method. Further details on the numerical procedure can be found in Bosch (1995).

Computational domain and boundary conditions

The computational domain and the boundary conditions are sketched in Figure 1. In addition, the location of the pressure transducer used in the experimental part of this study is indicated. A mesh with 106×75 cells was used as shown in Figure 2 for the gap $G_w/D = 0.5$.

At the inlet, the flow enters with only a streamwise component u_∞ and the experimental turbulence level of $Tu = u'/u_\infty = 4\%$ is prescribed. A ratio of $\nu_t/\nu = 10$ is assumed to compute the inflow value of the dissipation rate ε. In front of the wall ($x/D < -6$) at the bottom boundary, and at the top boundary a symmetry condition is used. At the outlet, a convective boundary condition is prescribed. On all solid boundaries the usual wall functions are employed to bridge the viscous sublayer. The first grid points from the walls were located in the region $16 \leq \bar{y}^+ \leq 50$.

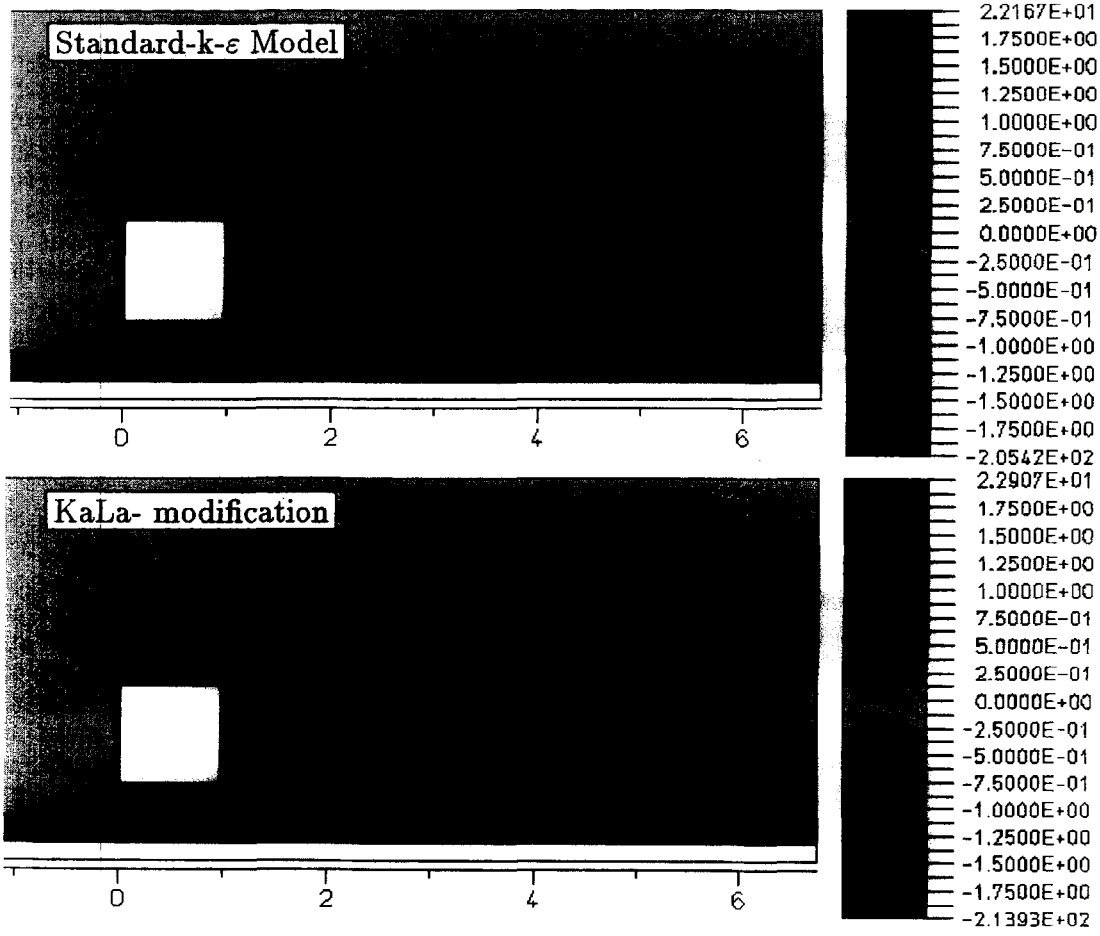

Figure 3 $\bar{\omega}$ for the standard k-ε model and the modification of Kato and Launder (1993) ($G_w/D = 0.5$)

Some calculations of the flow around a free-standing cylinder were carried out with a finer 140×106 mesh, but only small differences resulted to the solution on a grid with 99×75 cells, which was hence found appropriate.

Experiments

The measurements were carried out in a closed water tunnel. An additional wall was placed in the test section, close to one tunnel side wall, starting 26 cm in front of the cylinder centre. The effective tunnel cross section was 51×39 cm. The boundary-layer thickness at the location of the cylinder was $\delta/D = 0.1$, in the absence of the cylinder. The square cylinder spanned the whole height of the tunnel (39 cm) and had a width of $D = 4$ cm. The Reynolds number, $\mathrm{Re}_D = u_\infty D/\nu$ was chosen as $\mathrm{Re}_D = 22{,}000$, the same as in the experiments of Lyn et al. (1995). Preliminary flow visualisations were performed to study the global flow behaviour for different gap widths using a laser light sheet and a video camera perpendicular to the plane of the light sheet.

Velocity measurements with a two-channel LDV system were made at the central horizontal plane of the channel for $G_w/D = 0.75$. Ensemble-averaged statistical quantities at constant phase were obtained with the signal-processing method described in Lyn et al. (1995), with the phase defined by a pressure signal measured on the cylinder side face away from the wall (see Figure 1). The shedding period was divided into 12 discrete phases at which the phase-averaged velocities $\langle u \rangle$, $\langle v \rangle$ and Reynolds stresses $\langle u'^2 \rangle$, $\langle v'^2 \rangle$, $\langle u'v' \rangle$ were measured. Details on

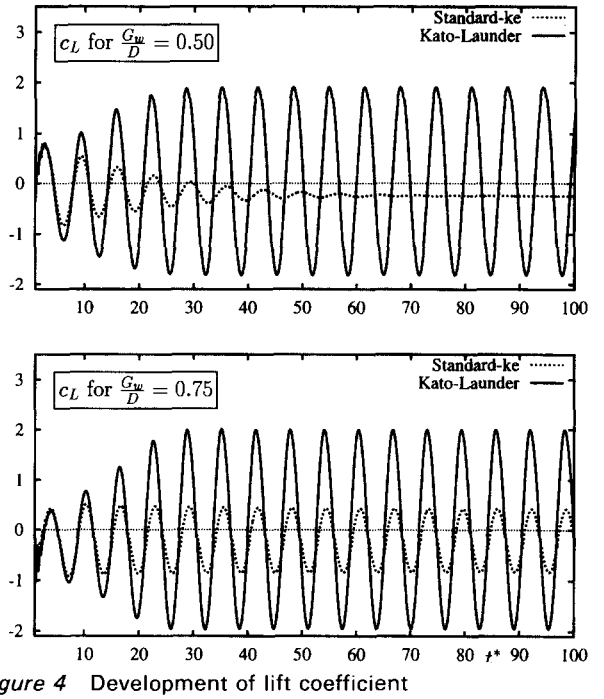

Figure 4 Development of lift coefficient

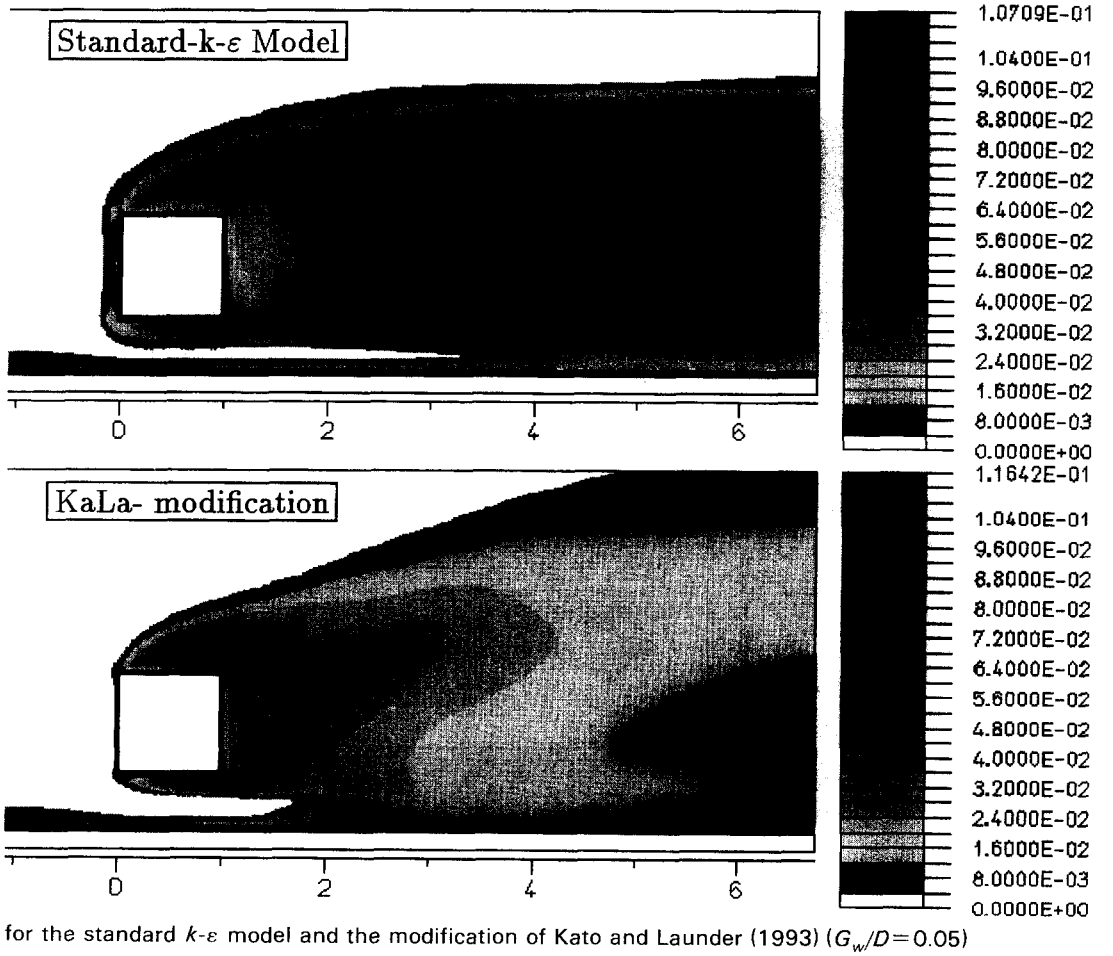

Figure 5 k for the standard k-ε model and the modification of Kato and Launder (1993) ($G_w/D = 0.05$)

the measurements are described in Kappler (1995), Bosch (1995) and Bosch et al. (1996).

Presentation and discussion of results

Square cylinder remote from wall

First, results are presented for the limiting case of the flow past a square cylinder remote from the wall to illustrate the influence of the turbulence model modification in this case and to compare the results with similar calculations carried out by Kato and Launder (1993). The case simulated is the one studied experimentally by Lyn et al. (1995) at Re = 22,000. In Table 1, results for the Strouhal number Str and the time-mean drag coefficient $\overline{c_D}$ are compared for various calculations with measurements. Results are included from calculations with both the standard k-ε model and the KaLa modification, using wall functions in both cases, the inflow plane being $4.5D$ upstream of the cylinder and $\nu_t/\nu = 100$ specified at inflow, as in the calculations of Franke and Rodi (1993). It can be seen from Table 1 that for both model versions, the present calculations agree fairly well with those of Kato and Launder, giving confidence in the numerical solution. It can also be seen that the predictions of Str and $\overline{c_D}$ are in much closer agreement with the measurements when the KaLa modification is used. It should be mentioned that Franke and Rodi did not obtain any vortex shedding with the standard k-ε model using wall functions. Bosch (1995) has shown that with the initial conditions used, the onset of vortex shedding takes a long time so that these authors' simulation duration may have been insufficient. Bosch has also found that the inflow boundary at $x/D = -4.5$ is too close to the cylinder, as the velocity and pressure field is already disturbed at this location and that $\nu_t/\nu = 10$ at inflow would be a more reasonable estimate for the experimental conditions of Lyn et al. In calculations starting at $x/D = -10$ with this inflow value he found a similar influence of the turbulence-model modification, but a lower value for $\overline{c_D}$ than given in Table 1. However, when resolving the viscous near-wall region in a two-layer approach, $\overline{c_D}$ was increased to the experimental level and, also, the total fluctuating energy was raised and is now closer to the measured level, a result obtained by Franke and Rodi only with the stress-equation model.

Comparison of standard k-ε model and Kato-Launder modification

For the case of $G_w/D = 0.5$, for which the present experiments indicated vortex shedding, the calculations with the standard k-ε model yielded a steady solution. The vorticity contours, which in this calculation are independent of time, are shown in Figure 3. For comparison the time-mean distribution of the vorticity $\overline{\omega}$ obtained with the KaLa modification is also given.

Figure 7 shows a sequence of phase-averaged vorticity contours for the calculations with the KaLa modification. This modification clearly produces vortex shedding in agreement with the experiments and, as can be seen from Figure 3, considerably smaller time-mean vortices.

The difference in model behaviour is also obvious from Figure 4 which compares the history of the lift coefficient c_L for $G_w/D = 0.5$ and 0.75. Because of the asymmetric nature of the

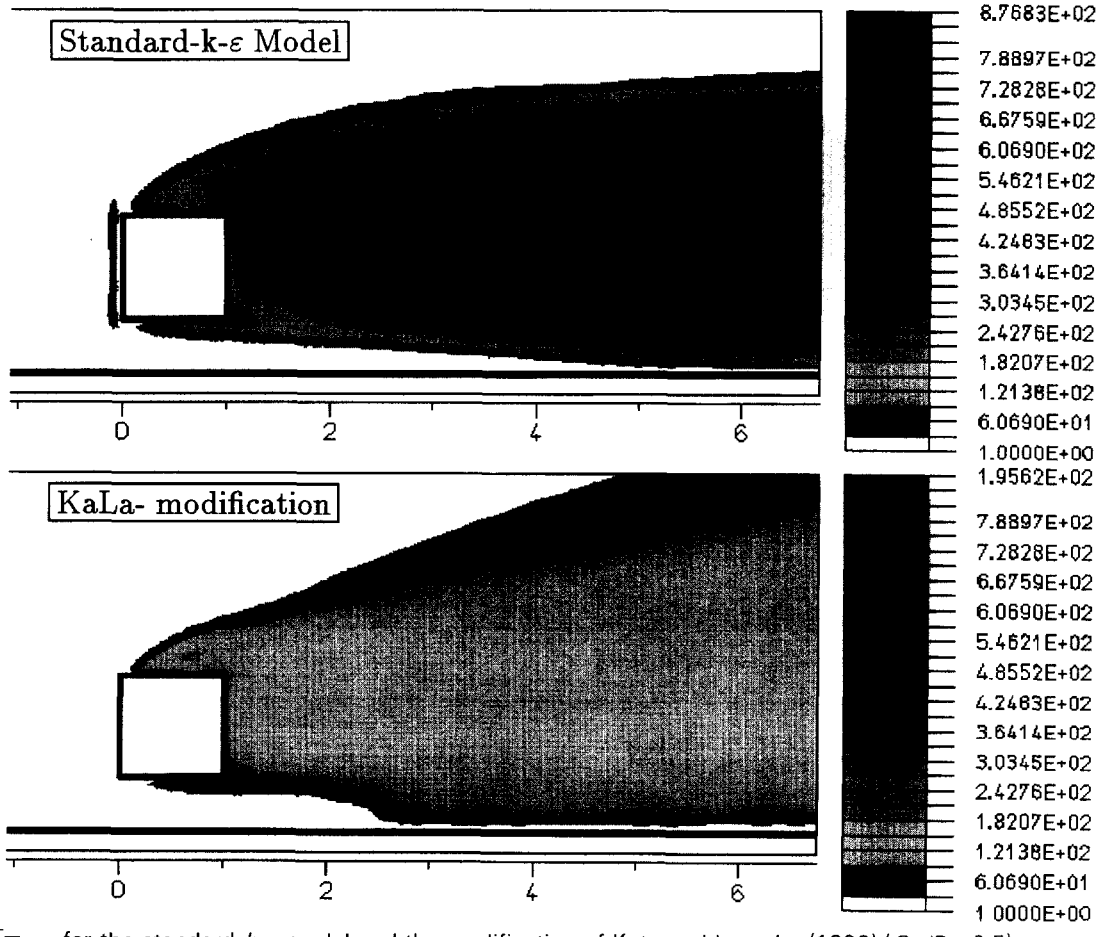

Figure 6 $\overline{r_\mu} = \nu_t \nu$ for the standard k-ε model and the modification of Kato and Launder (1993) ($G_w/D = 0.5$)

flow configuration and the symmetric initial conditions, there are large disturbances at the beginning, which result in an higher frequency oscillatory behaviour ($t^* < 3$). However, for $G_w/D = 0.5$ these disturbances are damped out when the standard k-ε model is used while, with the KaLa modification, vortex shedding results from these initial disturbances. For the increased gap width of $G_w/D = 0.75$ both model variants yield vortex shedding. However, with the standard k-ε model the shedding is much more damped. For $G_w/D = 0.25$ both model versions yields a steady solution in agreement with the experimental findings.

Figure 5 compares the time-averaged contours of the turbulent kinetic energy $\bar{k}$ calculated with the standard k-ε model and the KaLa modification for $G_w/D = 0.5$. The excessive level of k produced in front of the cylinder by the standard model can be clearly seen. This fairly high turbulence is swept around the cylinder and causes too high eddy-viscosity and, therefore, too much damping in the wake, preventing the occurrence of vortex shedding in this case. The excessive k-levels in the surroundings of the front stagnation point are suppressed by the KaLa modification and the resulting lower eddy-viscosity in the wake makes vortex shedding possible.

The time-mean distributions of the dimensionless eddy-viscosity $\overline{r_\mu} \equiv \overline{\nu_t}/\nu$ are compared for the two turbulence models in Figure 6. The levels in the wake can be seen to be quite different. Computing a Reynolds number with the maximum eddy-viscosity in the wake yields a value of $\mathrm{Re}_t = \mathrm{Re}_D \cdot \nu/\nu_t = 25$

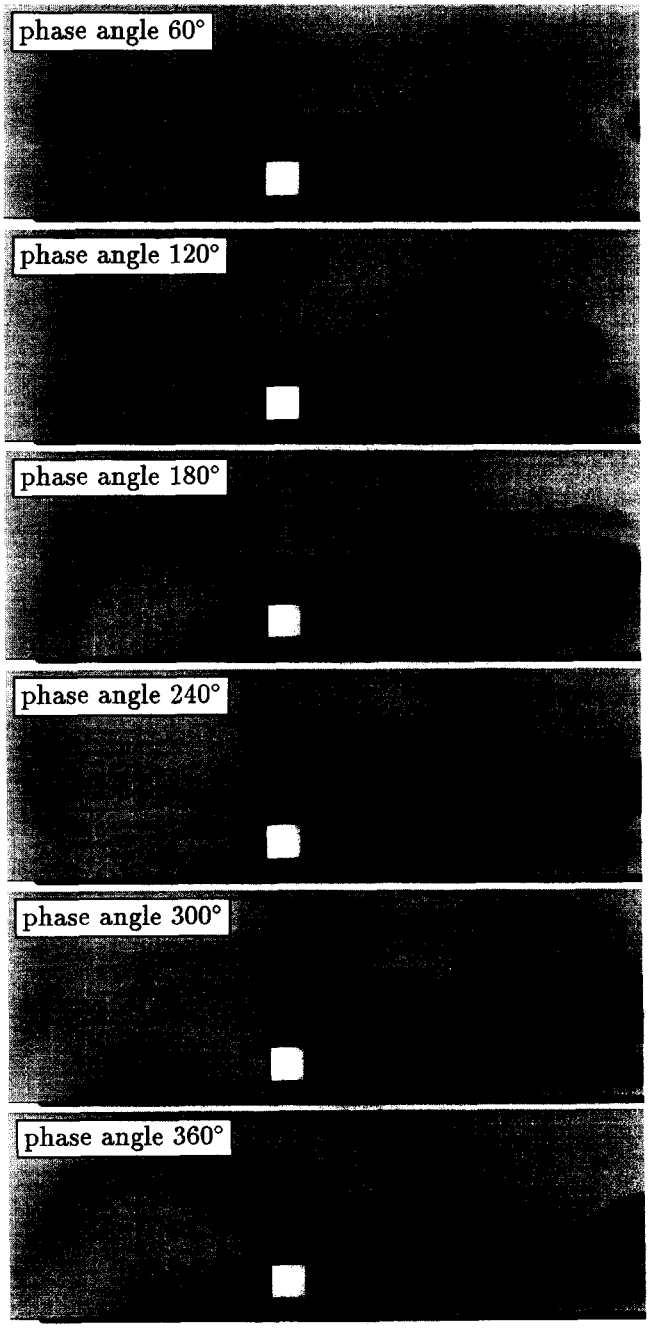

Figure 7 Vorticity contours at various phase angles ($G_w/D = 0.5$)

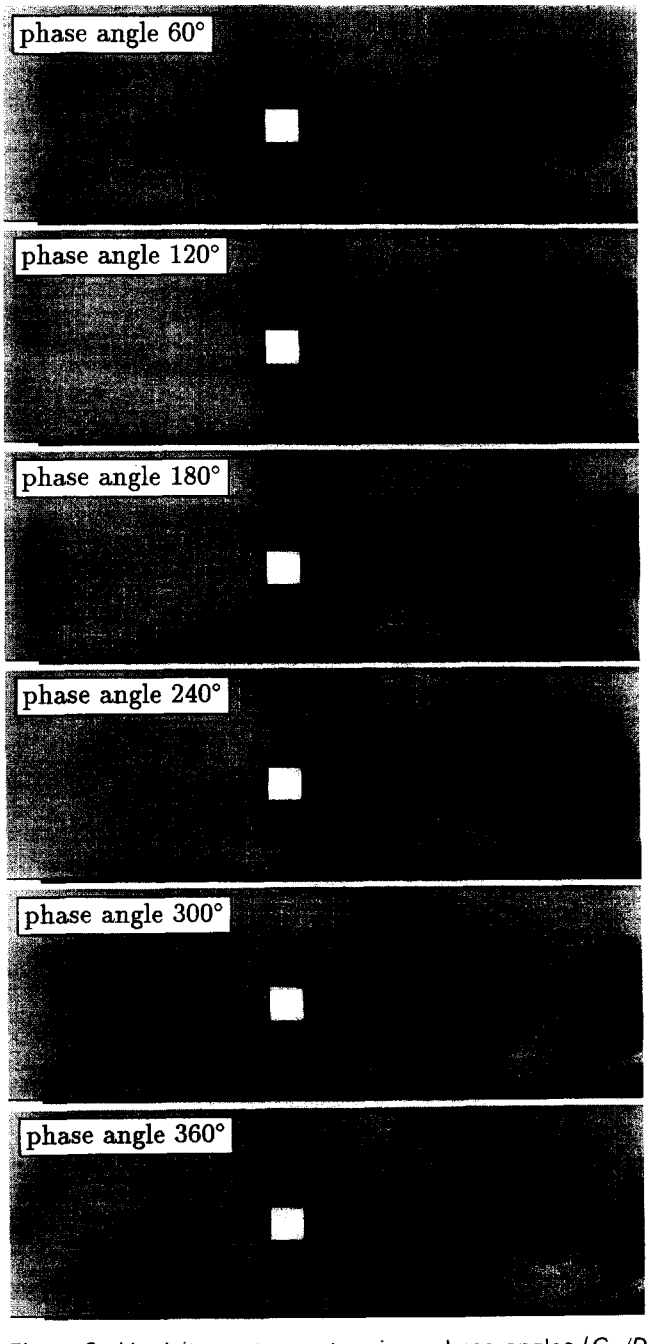

Figure 8 Vorticity contours at various phase angles ($G_w/D = 2.0$)

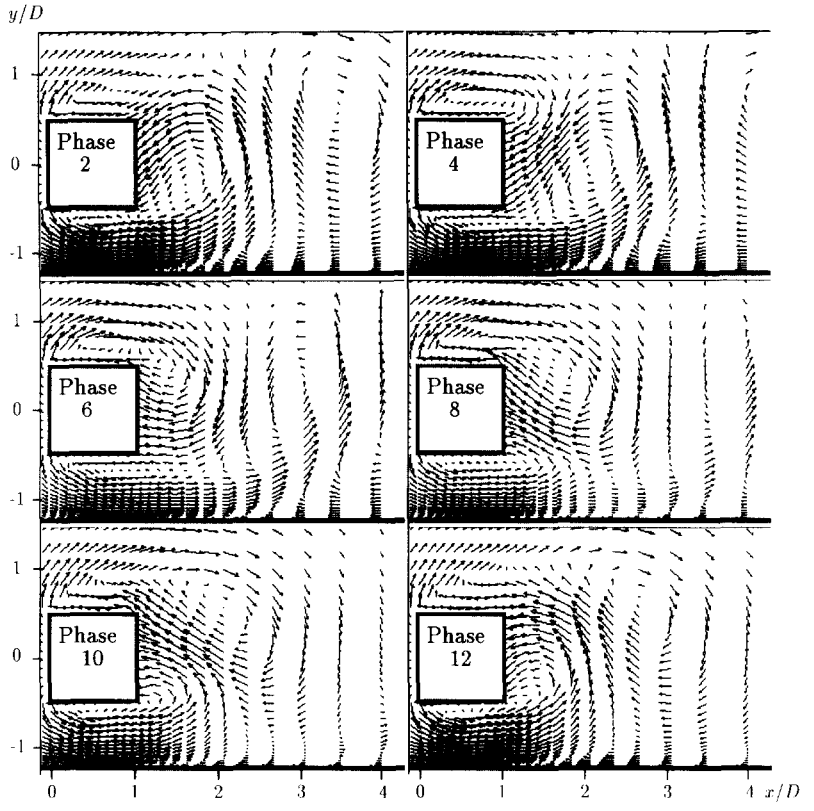

Figure 9 Calculated velocity vectors for $G_w/D=0.75$ with $u_B=0.68u_\infty$

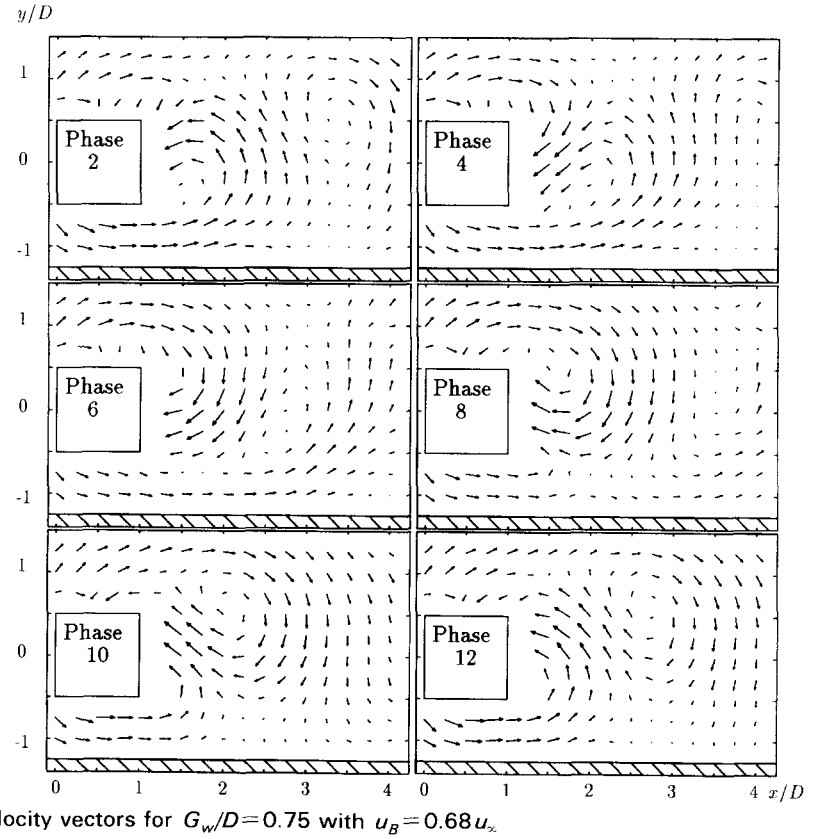

Figure 10 Measured velocity vectors for $G_w/D=0.75$ with $u_B=0.68u_\infty$

with $\overline{r_\mu}|_{max} = 876$ for the standard k-ε model and $Re_t = 112$ with $\overline{r_\mu}|_{max} = 196$ for the KaLa modification. The critical Reynolds number for the appearance of vortex shedding is given in the literature for a square cylinder remote from the wall as $Re_D^{critical} = 70$. This helps to explain why no vortex shedding is observed with the standard k-ε model.

Results at various phases

In the following, only calculations with the KaLa modification are presented. Figures 7 and 8 show calculated ensemble-average vorticity contours at six phase angles within one shedding period for $G_w/D = 0.5$ and 2.0, respectively. The shading table is the same as in Figure 3. The wall starts at $x/D = -6$, and the boundary layer developing on it can be seen as dark area representing fluid with strong vorticity. Discussing first the case with the smaller gap (Figure 7), in the second picture at phase 120° the vortex on the upper side is just shedding, while a counterrotating vortex is forming on the lower side behind the cylinder. Two counterrotating vortices that have shed already can be seen farther downstream. It is noteworthy that the vortex shed from the upper side is still strong and nearly circular, while the vortex shed from the lower side is smaller, weaker, and substantially stretched in the local flow direction; it is strongly influenced by the presence of the adjacent wall. The vortices forming on the upper side have clockwise rotation, and those forming on the lower side, counter-clockwise rotation; in the region where they are close to each other, there is a fairly strong upward motion which sucks the boundary layer into this region, a process seen even more clearly for 180°. Part of the boundary layer, having also vorticity with clockwise rotation, is then engulfed into the vortex shed from the upper side. At 180°, the vortex from the upper side has clearly separated from the cylinder, while the one from the lower side is just shedding. At 360°, the formation of the elongated vortex shed from the lower side can be seen, which accelerates and pushes down the boundary layer below it. At the same time, a new vortex forms on the upper side. Farther downstream it can be seen that the vortices shed from the lower side are much weaker and decay fairly quickly.

Moving now to the case with the larger gap ($G_w/D = 2.0$, Figure 8), it is clear that there is much less interaction between the vortex-shedding motion and the boundary layer. Still, the boundary layer is disturbed by this motion and thickens in regions between two counterrotating vortices, while it is thinned beneath the vortices themselves. On the other hand, the wall now has a much smaller influence on the shed vortices, because those shed from either side now have more-or-less the same strength and shape. In the first picture, the vortex is just shed from the upper side, while a new vortex forms on the lower side behind the cylinder. In the third picture, this vortex is shedding, while in the fifth picture, it has shed and a new vortex is forming on the other side.

Figure 9 shows the calculated ensemble-average velocity vectors for six different phases, and Figure 10 shows the measured velocity vectors at the same phases. In both cases, the flow field is shown with respect to an observer moving with the speed of $u_B = 0.68u_\infty$ in order to allow better visualisation of the vortices. At phase 4, a vortex separates from the lower side of the cylinder, and this vortex is carried downstream and away from the wall, as can be seen at phases 6 and 8. Between phase 6 and phase 8, a vortex is created on the upper side, which separates at phase 10. A new vortex created at phase 9 on the lower side then also separates at the next cycle of the vortex shedding. Comparing the velocity vectors in Figures 9 and 10, generally good agreement can be seen concerning the formation, the shedding, and the downstream transport of the vortices.

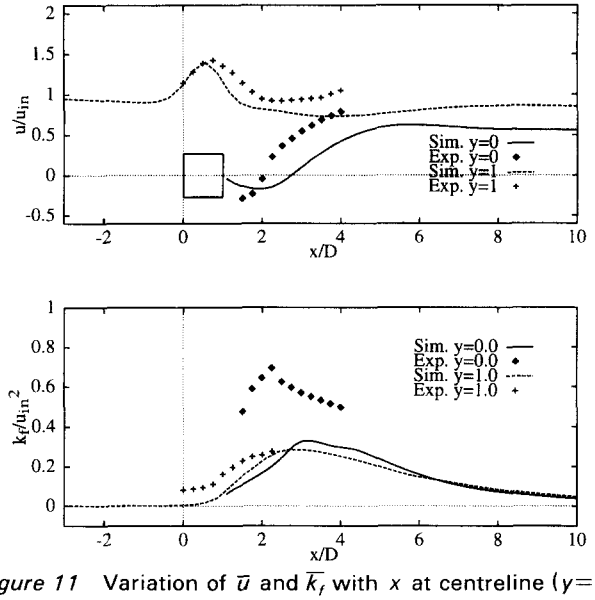

Figure 11 Variation of $\bar{u}$ and $\overline{k_f}$ with x at centreline ($y=0$) and $y=1D$

Comparison of time-mean quantities

Figure 11 compares the calculated and measured distribution with x of the time-mean velocity $\bar{u}$ and the time-mean total fluctuating energy $\overline{k_f}$ along the centreline of the cylinder ($y = 0$) and along the line $y = 1D$. At the centreline, the length of the separation region is overpredicted, and $\bar{u}$ does not rise fast enough, and not to the measured level. A similar behaviour was observed already for the cylinder remote from a wall (Bosch 1995) but could be remedied by the use of the two-layer approach resolving the near-wall viscous sublayer. At $y = 1D$, the distribution of $\bar{u}$ is first predicted in fairly good agreement with the measurement, but then the predicted velocity also settles at a lower value than observed. This discrepancy and, in particular, the continued increase in $\bar{u}$ in the measurements are difficult to understand. The total fluctuation energy (including periodic and turbulent fluctuations) shown in Figure 11 agrees fairly well between calculations and measurements at $y = 1D$, but at the cylinder centreline, the level of the predicted fluctuations is much too low. A similar trend was observed for the cylinder remote from the wall (Bosch 1995) and could again be remedied by resolving the viscous near-wall layer with a two-layer approach.

Conclusions

The main conclusion to be drawn from this study is that the modification of Kato-Launder (1993) improves significantly the predictions of vortex-shedding flow past a square cylinder also in the presence of an adjacent wall. While the standard k-ϵ model yields no shedding at smaller gap widths where shedding has been observed and causes the shedding motion at larger gap widths to be much too damped, the KaLa modification predicts transition from steady flow to vortex-shedding flow in the observed range of gap widths and appears to give reasonable predictions of the shedding motion for all gap widths. The sequences of vorticity contours presented have shown that the calculations allow the details of the interaction between the vortex-shedding motion and the boundary layer developing on the adjacent wall to be studied. For $G_w/D = 0.75$, a comparison

with the present measurements has shown that, overall, the flow is simulated quite well, but not all details are in full agreement with the measurements. Following the findings of Bosch (1995) for the flow past a cylinder remote from walls, it may be speculated that the results could be improved further by resolving the viscosity-affected near-wall region in a two-layer approach, at the expense of significantly increased computing cost.

Acknowledgments

The work reported here was sponsored by the Deutsche Forschungsgemeinschaft through the Sonderforschungbereich 210. The calculations were carried out on the SNI S600/20 computer of the University of Karlsruhe.

References

Bosch, G. 1995. Experimentelle und theoretische Untersuchung der instationären Strömung um zylindrische Strukturen. Ph.D. thesis, University of Karlsruhe, Karlsruhe, Germany

Bosch, G., Kappler, M. and Rodi, W. 1996. Experiments on the flow past a square cylinder placed near a wall. To appear in *Experimental Thermal and Fluid Science*

Durao, D. F. G., Gouveia, P. S. T. and Pereira, J. C. F. 1991. Velocity characteristics of the flow around a square cross section cylinder placed near a channel wall. *Exp. Fluids*, **11**, 298–304

Franke, R. and Rodi, W. 1993. Calculation of vortex shedding past a square cylinder with various turbulence models. In *Turbulent Shear Flows 8*, F. Durst et al. (eds.), Springer, New York, 189–204

Kappler, M. 1995. Experimentelle Untersuchung der instationären turbulenten Wirbelablösung an einem quadratischen Zylinder in einer Scherströmung und in Wandnähe. Diploma-Thesis, University of Karlsruhe, Karlsruhe, Germany

Kato, M. and Launder, B. E. 1993. The modelling of turbulent flow around stationary and vibrating square cylinders. *Proc. 9th Symposium on Turbulent Shear Flows*, Kyoto, Japan, 10–4

Lyn, D. A., Einav, S., Rodi, W. and Park, J.-H. 1995. A laser-Doppler velocimetry study of ensemble-averaged characteristics of the turbulent near-wake of a square cylinder. *J. Fluid Mech.*, **304**, 285–319

Majumdar, S., Rodi, W. and Schönung, B. 1989. Calculation procedure for incompressible three-dimensional flows with complex boundaries. In *Finite Approximations in Fluid Mechanics II*, *Notes on Numerical Fluid Mechanics*, Vieweg Verlag, Braunschweig

Rhie, C. M., Chow, W. L. 1983. A numerical study on the turbulent flow past an isolated airfoil with trailing-edge separation. *AIAA J.*, **21**, 1525–1532

Van Doormal, J. P. and Raithby, G. D. 1984. Enhancements of the SIMPLE method for predicting incompressible fluid flows. *Numer. Heat Transfer*, **7**, 147–163

Zhu, J. 1991. A low-diffusive and oscillation-free convection scheme. *Comm. Appl. Numer. Meth.*, **7**, 225–232